nature
photonics

ARTICLES

PUBLISHED ONLINE: 5 MAY 2013 | DOI: 10.1038/NPHOTON.2013.82

Polymer bulk heterojunction solar cells employing Förster resonance energy transfer

Jing-Shun Huang[1], Tenghooi Goh[1], Xiaokai Li[1], Matthew Y. Sfeir[2], Elizabeth A. Bielinski[3], Stephanie Tomasulo[4], Minjoo L. Lee[4], Nilay Hazari[3] and André D. Taylor[1]*

There are two crucial tasks for realizing high-efficiency polymer solar cells (PSCs): increasing the range of the spectral absorption of light and efficiently harvesting photogenerated excitons. Here, we describe Förster resonance energy transfer-based heterojunction polymer solar cells that incorporate squaraine dye. The high absorbance of squaraine in the near-infrared region broadens the spectral absorption of the solar cells and assists in developing an ordered nanomorphology for enhanced charge transport. Femtosecond spectroscopic studies reveal highly efficient (up to 96%) excitation energy transfer from poly(3-hexylthiophene) to squaraine occurring on a picosecond timescale. We demonstrate a 38% increase in power conversion efficiency to reach 4.5%, and suggest that this system has improved exciton migration over long distances. This architecture transcends traditional multiblend systems, allowing multiple donor materials with separate spectral responses to work synergistically, thereby enabling an improvement in light absorption and conversion. This opens up a new avenue for the development of high-efficiency polymer solar cells.

Polymer solar cells (PSCs) are promising candidates for providing low-cost, lightweight, large-area and mechanically flexible energy conversion devices[1–4]. Cells incorporating a binary bulk heterojunction (BHJ) blend based on regioregular poly(3-hexylthiophene) (P3HT) and [6,6]-phenyl-C$_{61}$-butyric acid methyl ester (PCBM) have been studied widely, providing power conversion efficiencies (PCEs) of 4–5% (refs 5–8). A critical step towards improving the PCE is to increase the quantum yields of incident photons. P3HT, with its bandgap of $\sim$2 eV, is only able to harvest 22% of the total photons in solar light[9,10]. A common route towards realizing broadband light harvesting makes use of low-bandgap polymers, which often require processing additives[11–14], making it difficult to precisely control both the crystallinity and phase separation of the photoactive layer. Additionally, the photogenerated excitons in the photoactive layer must reach the donor–acceptor interface to dissociate before recombination[4]. Unfortunately, an ideally bicontinuous interpenetration network is difficult to control[15], and results in $\sim$50% energy loss to recombination[16]. Recent studies in dye-sensitized solar cells have demonstrated that Förster resonance energy transfer (FRET) is a promising strategy to improve exciton migration over long distances[17–21]. Although it was thought that FRET may occur in P3HT–TiO$_2$ nanostructured solar cells featuring squaraine dye[22], to the best of our knowledge, experimental evidence that FRET can enhance exciton harvesting in polymer BHJ solar cells has never been presented. Furthermore, several groups have studied ternary-blend PSCs that utilize a third material[23] to either extend the solar spectrum[24–29] or control the phase separation[30]. In many cases, however, the third material in PSCs, such as porphyrin-based dye, has even reduced device performance through the formation of recombination centres and/or detrimental effects on blend morphology[24,25].

In this Article, we demonstrate, for the first time, efficient FRET in BHJ PSCs by incorporating 2,4-bis[4-(*N*,*N*-diisobutylamino)-2,6-dihydroxyphenyl] squaraine (SQ) in P3HT:PCBM blends to improve both the photon absorption range and exciton harvesting. Unlike common multiblend systems, FRET-based systems enable the effective use of multiple donors, thereby bringing significant improvements in light absorption and conversion. Femtosecond fluorescence and transient absorption (TA) spectroscopy on the ternary blends show energy transfer efficiencies of up to 96% (within the first few picoseconds) due to the large spectral overlap between the P3HT emission and SQ absorption. In addition to FRET, the SQ functions as a long-wavelength absorber due to its high absorbance ($\sim 3 \times 10^5$ M^{-1} cm^{-1}) in the red and near-infrared (NIR) spectral regions[31,32]. Both processes enhance the overall photocurrent in the resulting solar cells and we show that a nanomorphology with an interpenetrating network is well developed by SQ. As a result, the overall PCE is dramatically improved from 3.27% to 4.51%.

Optical characterization of P3HT and SQ

The molecular structures and optical properties of the materials used in this study are shown in Fig. 1. The P3HT absorption shows a broad spectrum from 400 to 650 nm with a peak at 515 nm and two shoulders at 550 and 600 nm. The vibronic feature at 600 nm indicates a high degree of ordered crystalline lamellae in the P3HT film due to strong interchain interactions[33]. The SQ dye has a high extinction coefficient of $\sim 3 \times 10^5$ M^{-1}cm^{-1} at 647 nm corresponding to π–π* charge transfer transitions. The cooperative absorption of P3HT and SQ covers a significant portion of the solar spectrum, with only limited overlap. This ensures that the addition of SQ will not inhibit the light absorption of the P3HT. Furthermore, the absorption of SQ strongly overlaps with the photoluminescence of P3HT, making these two materials a good FRET pair.

FRET is a non-radiative energy transfer process that acts through long-range dipole–dipole interactions between donor and acceptor molecules[34]. The strength of this interaction is strongly dependent on the overlap integral of the donor emission (P3HT) and the acceptor absorption (SQ) and can be summarized by the Förster

---

[1]Department of Chemical and Environmental Engineering, Yale University, New Haven, Connecticut 06511, USA, [2]Center for Functional Nanomaterials, Brookhaven National Laboratory, Upton, New York 11973, USA, [3]Department of Chemistry, Yale University, New Haven, Connecticut 06511, USA, [4]Department of Electrical Engineering, Yale University, New Haven, Connecticut 06511, USA. *e-mail: andre.taylor@yale.edu

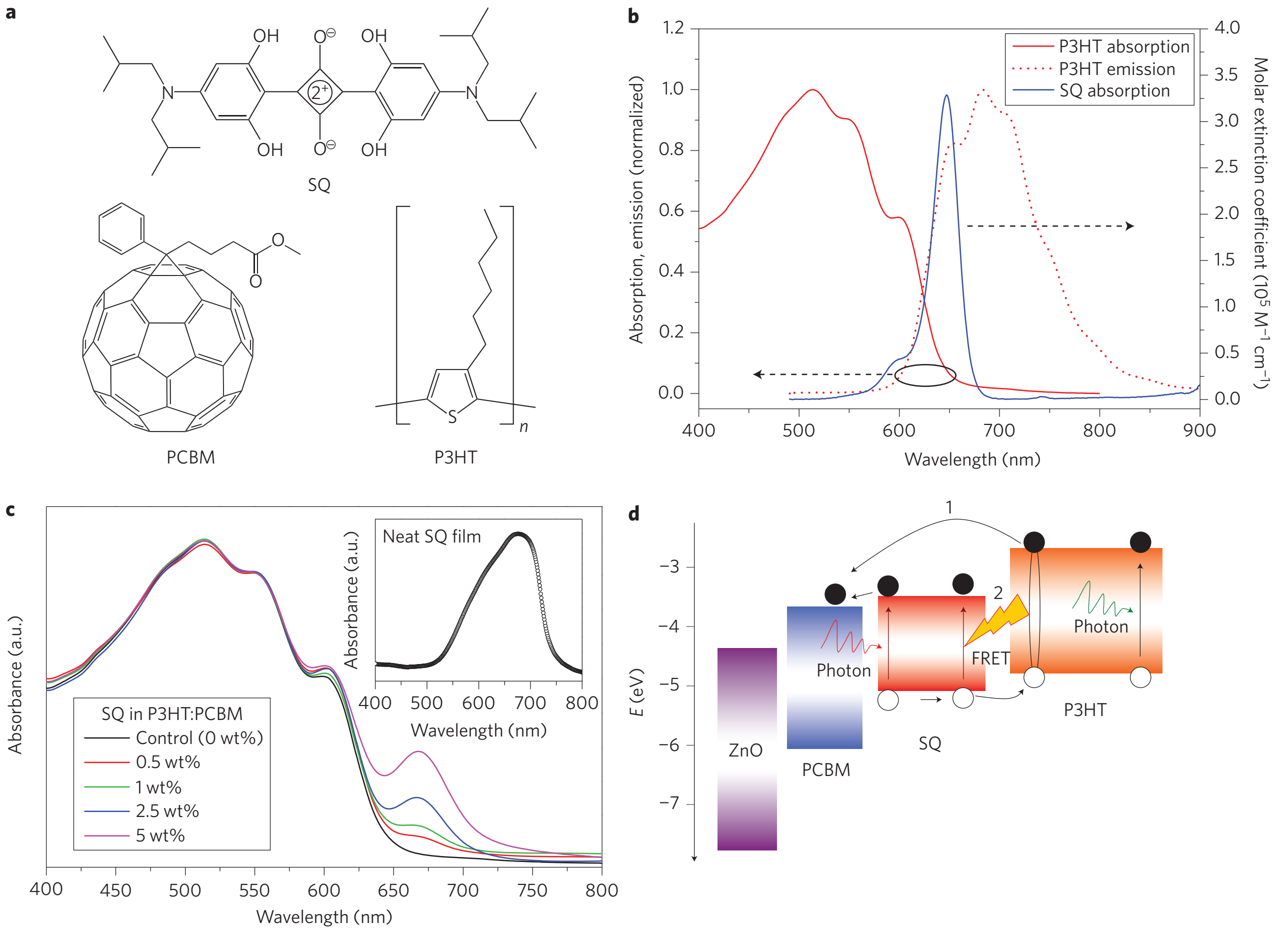

Figure 1 | P3HT and SQ properties. **a**, Chemical structures of SQ, PCBM and P3HT. **b**, Extinction coefficient (blue line) of SQ in 1,2-dichlorobenzene, and absorption (red solid line) and emission (red dotted line) spectra of P3HT film. **c**, Absorption spectra of P3HT:PCBM:SQ ternary blend films with various concentrations of SQ. Inset: absorption spectrum of neat SQ film. **d**, Energy level diagram of the components of the ternary blend solar cell highlighting pathways for charge generation.

radius R_0, the donor–acceptor separation distance where FRET is 50% efficient:

$$R_0 = 9.78 \times 10^2 \left[\frac{\kappa^2 Q_D}{n^4} \int F_D(\lambda) \varepsilon_A(\lambda) \lambda^4 \mathrm{d}\lambda \right]^{1/6} \text{(in nm)} \qquad (1)$$

where κ is the orientation factor between donor and acceptor dipoles, Q_D is the donor photoluminescence quantum efficiency, n is the refractive index, F_D is the donor emission spectrum and ε_A is the molar extinction coefficient of the acceptor[34,35]. We assume a random orientation of the donor and acceptor molecules ($\kappa^2 = 2/3$), an effective n of 1.4 and a Q_D of 1% for P3HT[36]. We calculate a Förster radius of 8 nm based on the spectral overlap integral from the normalized P3HT photoluminescence and SQ absorption spectra. The length of the Förster radius suggests that FRET will almost certainly occur between P3HT and SQ, provided the domain size of P3HT is less than 16 nm.

We show the optical absorption spectra of the P3HT:PCBM:SQ ternary films with various SQ concentrations (0–5 wt%) (Fig. 1c). All films were made on ZnO/glass substrates with the same procedures used for fabricating devices. To precisely assess the changes of absorption profiles and intensities upon the addition of SQ, the thickness of the films was monitored and held constant at ~200 nm. There are no obvious differences in the films regardless of the SQ loading between 400 and 575 nm. When the SQ loading increases, a growing peak appears at 675 nm, arising from SQ absorption. Furthermore, the shape of the P3HT peaks remains unchanged and the vibrational band at 600 nm (indicative of the P3HT crystallinity) is clearly observed and becomes slightly more pronounced (Fig. 1c). This implies that the interchain ordering of P3HT is not disturbed but improved by the addition of SQ.

An energy diagram outlining the possible pathways to current generation after excitation of P3HT and SQ is shown in Fig. 1d. The highest occupied molecular orbital (HOMO) level of SQ is located between the HOMOs of P3HT and PCBM[32]. The same is true for the lowest unoccupied molecular orbital (LUMO) levels. As a consequence, the photoinduced charge transfer is energetically favourable between P3HT and PCBM, and also between SQ and PCBM (Supplementary Figs S1, S2). Another possible energy transfer route is FRET of the P3HT excitation to SQ and subsequent charge dissociation. We note that in general for a P3HT:PCBM binary film, only one pathway (1) can contribute to charge transfer, while incorporating SQ introduces another route (2), implying that more excitons can be harvested in this ternary blend system.

Photophysics study of P3HT and SQ

To experimentally verify the hypothesis of FRET occurring between P3HT and SQ, we examined the photoluminescence spectra of P3HT-only, SQ-only and several P3HT/SQ co-solutions with varying SQ content, in 1,2-dichlorobenzene. We compared the photoluminescence spectra of the samples excited at 525 nm (Fig. 2a). As the SQ content increases, the emission from P3HT significantly decreases while the SQ emission continuously increases. We note that a very weak emission is detected for a SQ-only

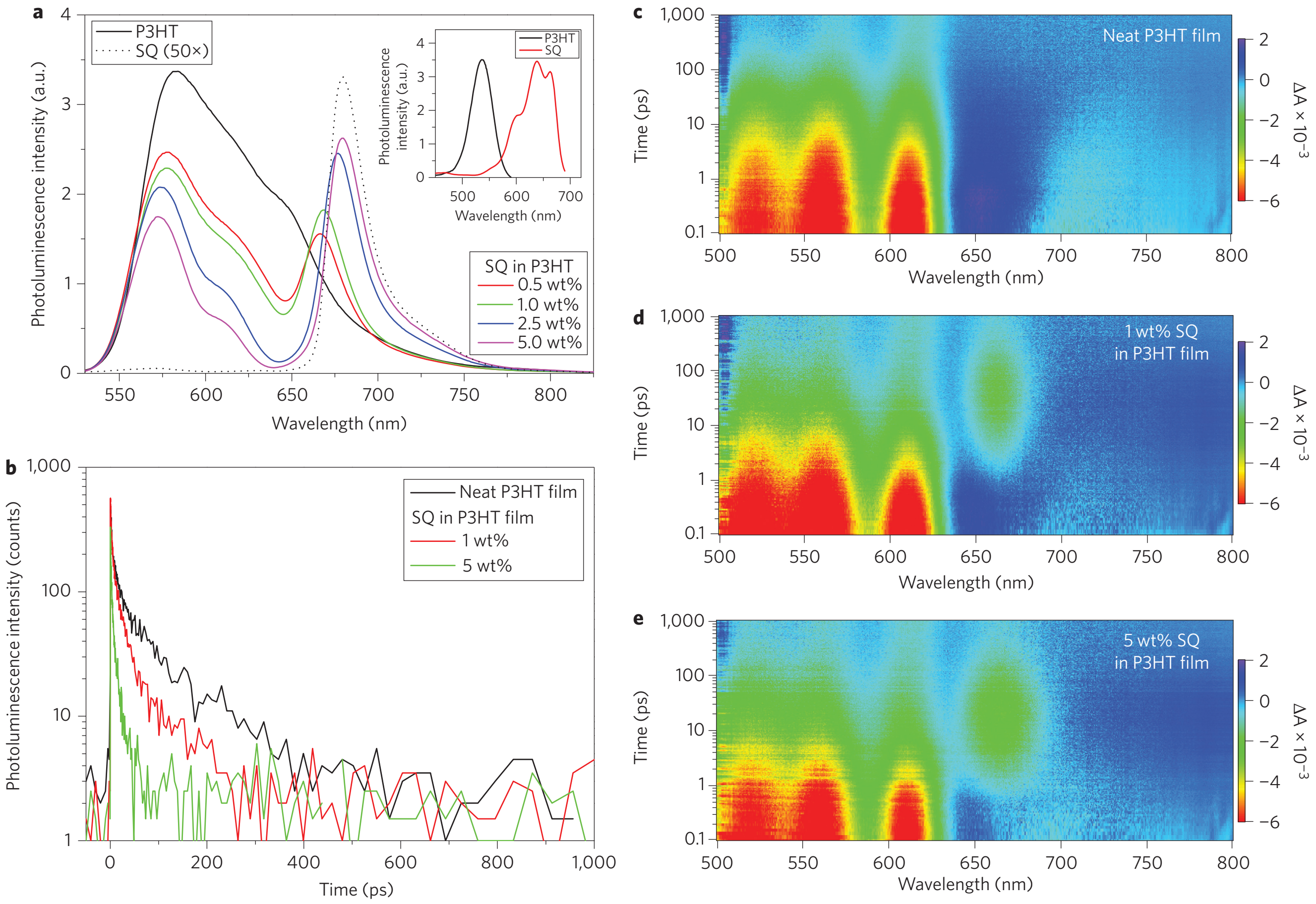

Figure 2 | Photophysical study. **a**, Emission spectra (pumping wavelength, 525 nm) of neat P3HT solution (black solid line), neat SQ solution (black dotted line) and P3HT/SQ co-solutions with SQ ratio from 0.5 to 5 wt%. Inset: photoluminescence excitation spectra of neat P3HT solution (black) and neat SQ solution (red). The excitation spectrum of neat P3HT was obtained at an emission wavelength of 600 nm, and that for neat SQ was obtained at 700 nm. **b**, Time-resolved decay traces of neat P3HT film, and P3HT:SQ blend films with 1 and 5 wt% SQ. **c**–**e**, TA spectra of neat P3HT (**c**), P3HT:SQ with 1 wt% SQ (**d**) and 5 wt% SQ (**e**). The pumping wavelength in **b**–**e** was 500 nm with a fluence of 8 μJ cm^{-2}.

solution, because there is minimal absorption by SQ at this excitation wavelength. We also show the excitation spectra of the two individual molecules, further confirming that at the excitation wavelength of 525 nm, there is negligible excitation of the SQ. However, there is significant excitation of P3HT (Fig. 2a, inset). As direct photoexcitation is not occurring, emission from the SQ can only occur if it is being photoexcited by near-field interactions with the P3HT.

Förster theory predicts a decrease in the excited-state lifetime of the FRET donor with increasing FRET acceptor concentrations, as FRET introduces an additional non-radiative decay path for the donor into the system[34]. We probed the fluorescence decay of P3HT dynamics as a function of SQ concentration by applying the femtosecond fluorescence upconversion technique (Fig. 2b). The samples were pumped at 500 nm and probed at 690 nm. In the absence of SQ, the average lifetime of a neat P3HT film was 223 ps and decreased to 52.4 ps with the addition of 1 wt% SQ, and further to 9.9 ps with 5 wt% SQ. The efficiency of energy transfer E can be calculated using the formula[34]

$$E = 1 - \frac{\tau_{\mathrm{DA}}}{\tau_{\mathrm{D}}} \tag{2}$$

where τ_{D} and τ_{DA} are the fluorescence lifetime of the donor in the absence and presence of the acceptor, respectively. From this time-dependent data, we obtain a transfer efficiency of 77% for 1 wt% SQ and 96% for 5 wt% SQ.

To monitor the photophysical processes of P3HT and SQ simultaneously, we used TA spectroscopy. We show the time- and spectrally resolved TA spectra of P3HT:SQ films with 0, 1 and 5 wt% SQ, respectively (Fig. 2c–e). Three films were excited at 500 nm to selectively excite P3HT. The laser fluence was set to 8 μJ cm^{-2}, which is within the linear response of the TA signal of P3HT. We illustrate the typical features of the P3HT film (Fig. 2c). At early times (<10 ps), the negative signal containing three peaks at 520, 560 and 610 nm corresponds to the P3HT absorption with 0–2, 0–1 and 0–0 vibrational transitions, respectively, representing the ground-state bleach (GSB) of P3HT. In addition, the P3HT GSB exhibits a prominent 0–0 vibronic feature that indicates a good degree of P3HT ordering, even in the presence of SQ. This again confirms that P3HT ordering is not disturbed by SQ. The positive signal (blue in colour) at 650 nm represents the photoinduced absorption of the excited states in the P3HT. Another negative signal beyond 700 nm is associated with stimulated emission of P3HT. Introducing 1 or 5 wt% SQ causes a sign change of the TA signal at 665 nm (colour from blue to green in Fig. 2d,e). This negative signal is identified as the GSB of SQ, indicating that the SQ is being excited. Because the SQ had negligible absorption at 500 nm, the excitation of SQ is almost certainly not caused by the pumping wavelength but by the excited P3HT. Meanwhile, signals of the photoinduced absorption and stimulated emission in P3HT both substantially decayed to zero. These findings indicate that the excitation energy is successfully transferred from the P3HT to the SQ.

Table 1 | Summary of photovoltaic parameters and efficiencies of BHJ blend solar cells with various concentrations of SQ.

SQ concentration (wt%)	Efficiency (%)	V_{OC} (V)	J_{SC} (mA cm^{-2})	FF (%)	R_S (Ω cm^2)	R_{SH} (Ω cm^2)
0 (control)	3.27	0.59	10.3	53.0	7.50	769
0.5	3.48	0.59	11.0	53.6	4.81	904
1	4.51	0.60	11.6	64.8	2.87	941
2.5	3.92	0.59	11.9	55.8	4.12	740
5	3.93	0.60	12.2	53.6	6.32	472

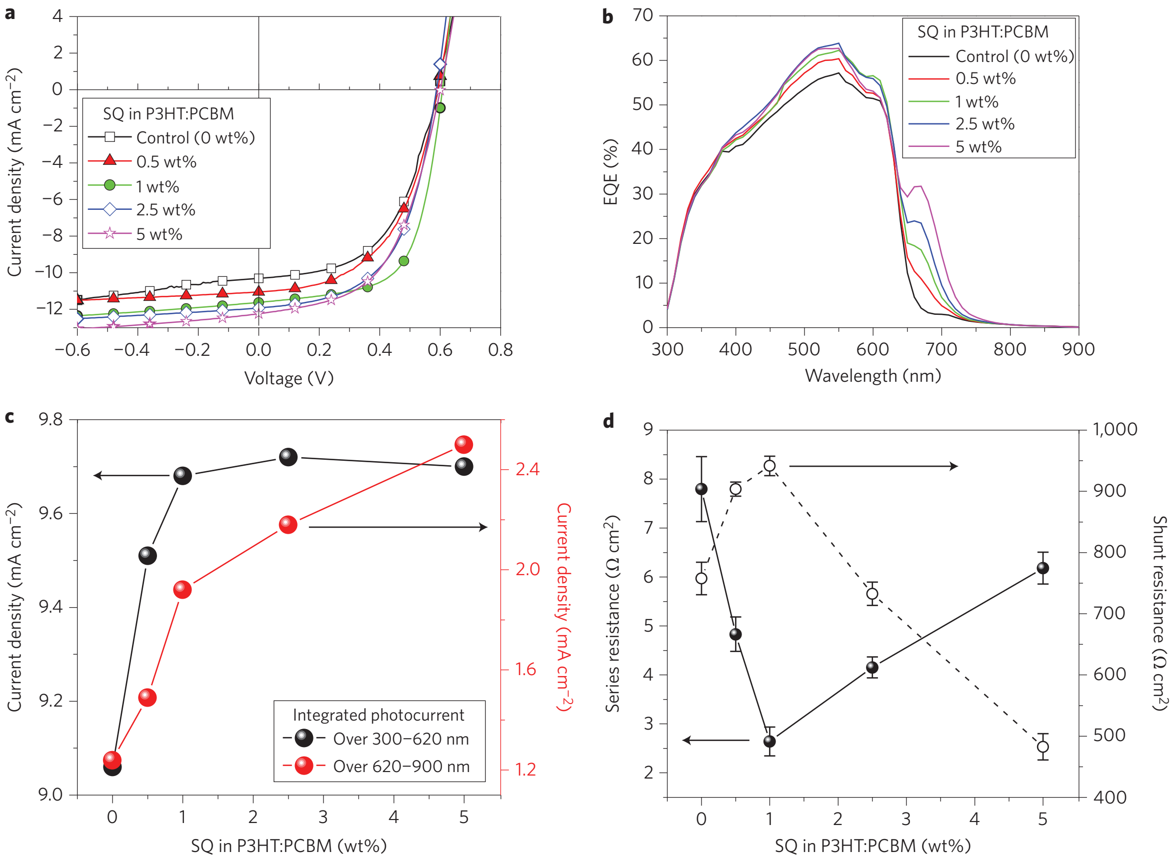

Figure 3 | Photovoltaic performance. a, *J–V* curves of the photovoltaic devices with SQ concentrations ranging from 0 to 5 wt% under 100 mW cm^{-2} AM 1.5G irradiation. **b**, EQE versus wavelength of devices with SQ concentrations ranging from 0 to 5 wt%. **c**, Photocurrents generated from spectral regions of 300–620 nm (black symbols) and 620–900 nm (red symbols) as a function of SQ concentration. The increase in the former was caused by FRET (visible region) and in the latter by SQ absorption (NIR region). **d**, Series and shunt resistance as a function of SQ concentrations in the ternary BHJ layer. Data were taken for six different devices.

The GSB of SQ is observed almost immediately after excitation (∼1 ps), revealing a rapid energy transfer of excitons from P3HT to SQ. This was confirmed by evaluating the TA dynamics with a global fitting procedure via singular-value decomposition (Supplementary Fig. S3). At early times, both samples with SQ show positive amplitude coefficients (at 2.8 ps for 1 wt% SQ and at 0.6 ps for 5 wt% SQ) at 665 nm (indicating a rise of the SQ GSB feature), and negative values in the region from 500 to 620 nm (indicating a corresponding decay in the P3HT excited-state population). This behaviour is also linked to the excitation energy transfer from P3HT to SQ.

Photovoltaic performance

We show the current density–voltage (*J–V*) characteristics under one sun illumination (simulated AM 1.5G irradiation at 100 mW cm^{-2}) (Fig. 3a). Device performance parameters are summarized in Table 1. Control devices fabricated from P3HT:PCBM blend solutions have a typical PCE of 3.27%, with a short-circuit current density (J_{SC}) of 10.3 mA cm^{-2}, an open-circuit voltage (V_{OC}) of 0.59 V and a fill factor (FF) of 53%. Incorporating SQ in quantities of 0.5, 1, 2.5 and 5 wt% in the P3HT:PCBM film led to significant enhancements in the J_{SC} and FF values compared to the control device. Films with 1 wt% SQ in the ternary blend resulted in the highest PCE of 4.5%. Of the more than 50 devices that were evaluated, the best device displayed a J_{SC} of 11.6 mA cm^{-2}, V_{OC} of 0.6 V and FF of 64.8%. The average PCE was 4.35 ± 0.01% (Supplementary Table S1). Indeed, 90% of the optimum devices (with 1 wt% SQ) gave PCE values over 4.2% (Supplementary Fig. S4). When the loading of SQ was increased above 1 wt%, the J_{SC} monotonically increased while FF decreased. At 5 wt%, the PCE was 3.9%, which is still higher than the value of the control film.

We illustrate that the increase in J_{SC} corresponds to enhancements in the external quantum efficiency (EQE) (Fig. 3b). The devices with SQ show the typical spectral responses of P3HT (550 nm) and SQ (670 nm). The EQE spectra are consistent with

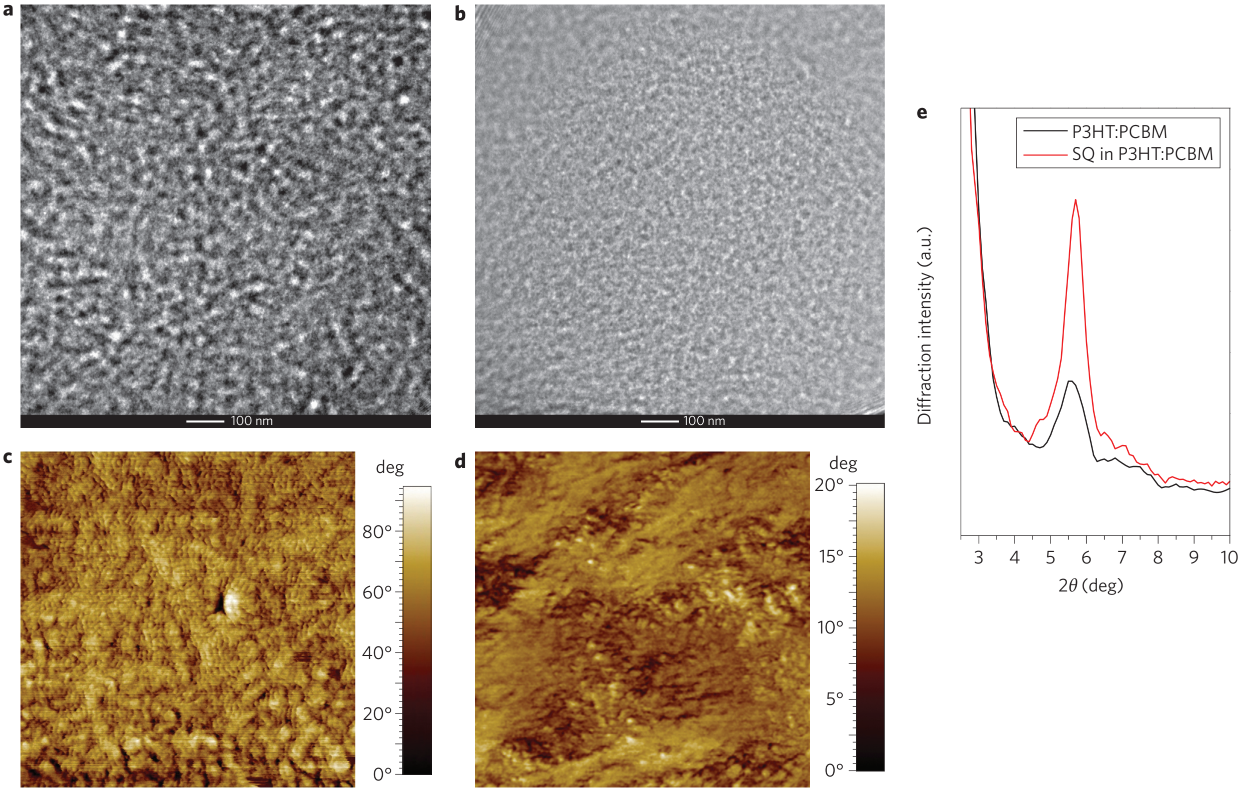

Figure 4 | Effects of 1 wt% SQ on morphology and crystallinity. a,**b**, TEM images of P3HT:PCBM with (**a**) and without (**b**) 1 wt% SQ. **c**,**d**, Tapping-mode AFM phase image of P3HT:PCBM with (**c**) and without (**d**) 1 wt% SQ. Image size is 1 μm × 1 μm. **e**, XRD spectra of P3HT:PCBM with (red line) and without (black line) 1 wt% SQ.

the measured J_{SC} in the devices. The enhancements in EQE can be divided into two regions, 300–620 nm and 620–900 nm. To pinpoint the SQ contribution spectrally, we compare the photocurrents in these two regions as a function of SQ concentration calculated from the EQE and AM 1.5G solar flux spectra. We show that the photocurrent in the 300–620 nm region increased from 9.06 mA cm^{-2} at 0 wt% to 9.68 mA cm^{-2} at 1 wt%, and then gradually saturated at 9.70 mA cm^{-2} at 5 wt% (Fig. 3c). For the control device, the photocurrent is generated by excitons in the P3HT and then dissociation at the P3HT–PCBM interfaces. Hence, the increase in this region is attributed to the additional excitons transferred to SQ and then dissociated into free charges, revealing that the excitons are harvested via FRET. The photocurrent in the 620–900 nm region gradually increases from 1.24 mA cm^{-2} (0 wt%) to 2.5 mA cm^{-2} (5 wt%) and we attribute this to the SQ absorption with a peak at 670 nm. The EQE spectra in the NIR region are consistent with the absorption spectra (Fig. 1c), revealing efficient harvesting of the NIR photons by SQ.

We compared the series resistances (R_S, defined from the J–V curves near 1.5 V under light illumination) and shunt resistances (R_{SH}, defined from the J–V curves near 0 V under light illumination) as a function of SQ concentration (Fig. 3d). The average R_S abruptly decreased from 7.8 to 2.6 Ω cm^2 at 1 wt% SQ loading, and then increased to 6.2 Ω cm^2 at 5 wt%. However, in all cases the R_S was lower in devices with SQ compared to the control device. This agrees with the dark J–V curves (Supplementary Fig. S5), where higher dark injection currents were observed for devices with SQ compared to the control device. In contrast, the average R_{SH} reached a maximum of 942 Ω cm^2 at 1 wt% SQ, while that in the control was only 758 Ω cm^2. It is known that the high R_{SH} indicates less leakage current across the cell and contributes to the improved FF. Interestingly, in an analogous fashion to the R_S, the R_{SH} and FF improved when the SQ loading was increased from 0.5 wt% to 1 wt%, and then decreased when the loading was further increased from 1 wt% to 5 wt%. This finding suggests that there is an optimal SQ loading and the effect decreases at high levels of SQ within the range investigated.

Study of nanomorphology

The improved FF is attributed to a lower R_S and an elevated R_{SH}, implying better nanoscale crystallinity and improved nanomorphology in the BHJ blends with SQ. Bright-field transmission electron microscopy (TEM) was used to investigate the differences in nanomorphology in the presence of SQ. The defocused phase contrast TEM images of P3HT:PCBM with and without SQ are presented in Fig. 4a,b, respectively. By properly defocusing, the image contrast can be significantly increased[37]. Both images were taken at a defocus close to −1 μm. It can be seen that the SQ alters the nanomorphology of the BHJ blend. The film without SQ shows a relatively smooth morphology, whereas the BHJ film with SQ shows a markedly different morphology with a feature size of ~20 nm. This interpenetrating network has dimensions comparable to approximately double the Förster radius R_0 (8 nm), consistent with the possibility of FRET. Atomic force microscopy (AFM) phase images of blend films with and without 1 wt% SQ are shown in Fig. 4c,d. The film preparation conditions for AFM images were the same as those for device fabrication so as to enable accurate comparison. In the phase images, highly ordered fibrillar crystalline domains of P3HT are visible in the blend film with SQ (Fig. 4c), but are absent in the film without SQ (Fig. 4d). In addition, studies of energy-dispersive X-ray elemental mapping and surface energy suggest that the SQ molecules prefer to reside at the P3HT/PCBM interfaces (Supplementary Fig. S6), thus enhancing the phase separation in ternary BHJ blends.

We note that the AFM and TEM observations are in agreement with the X-ray diffraction (XRD) spectra (Fig. 4e). Introducing 1 wt% SQ promoted an increase in the diffraction peak at $2\theta = 5.7^{\circ}$ (corresponding to the interchain spacing in P3HT[6]), showing that crystalline fibrils consisting of a more ordered packing of P3HT chains were formed by SQ. We suggest that the changes in morphology introduced by SQ lead to well-organized interpenetrating nanodomains and hence enlarge the donor/acceptor interfacial area for more efficient generation of charge carriers. From the above AFM, TEM and XRD studies, the resulting structural influences of SQ in BHJ blends are seen to be similar to those found from annealing treatments[7]. To our surprise, although the crystallinity of P3HT is enhanced by SQ, the fluorescence lifetime of P3HT is shortened from 223 ps to 52.4 ps for 1 wt% SQ, as mentioned in Fig. 2b. This reveals that the photophysical effects of SQ are quite different from those of annealing treatments, which usually bring about enhanced photoluminescence[33,38], elongated fluorescence lifetime[39,40] or charge-transfer time[41]. Presumably, this unusual phenomenon of enhanced crystallinity but shortened lifetime can be attributed to the strong energy transfer from excited P3HT to SQ.

In summary, we have successfully constructed BHJ solar cells incorporating SQ that show enhanced efficiency. In comparison to control devices, the device with 1 wt% SQ exhibited a significant increase of 38% in PCE due to improved J_{SC} and FF. Ultrafast TA experiments suggest that the use of FRET as a tool to broaden the spectral response is very efficient. Furthermore, the optimum SQ loading of 1 wt% is too small to obstruct the ordering of P3HT. Hence, it could be possible to further increase the photocurrent by incorporating other SQ molecules with different end-groups to broaden the absorption range deep into the NIR region. For instance, SQ with an aryl end-group can shift the absorption peak from 675 to 720 nm (ref. 32). In the future, the realization of a single-junction cell with a PCE beyond 10% might be possible by adopting FRET in other polymer systems, such as poly[*N*-9′-heptadecanyl-2,7-carbazole-alt-5,5-(4′,7′-di-2-thienyl-2′,1′,3′-benzothiadiazole)] (PCDTBT) or thieno[3,4-*b*]thiophene/benzodithiophene polymers (PTB7), for which PCEs have reached 7–9%. This architecture opens up a new paradigm towards significant improvements in the performance of PSCs.

Methods

Photovoltaic materials and devices. SQ dye was synthesized according to procedures described in the literature[42]. Supplementary Fig. S7 shows the ^{1}H NMR spectrum of SQ. Regioregular P3HT (Rieke Metals) and PCBM (Nano-C) were used as received. Devices were fabricated on cleaned indium tin oxide (ITO)-coated glass substrates (15 Ω sq^{-1}). A ZnO thin film (~50 nm) was spin-coated on ITO substrates using a sol–gel process. Subsequently, a ternary blend layer of P3HT:PCBM:SQ (~200 nm) was spin-coated on the ZnO thin film in a N_2-filled glovebox. The wet film was then dried in covered Petri dishes for 30 min. Finally, a silver film (~120 nm) was deposited on top in a vacuum of 5×10^{-7} torr. Pristine P3HT, PCBM and SQ solutions were separately prepared in 1,2-dichlorobenzene and mixed appropriately in an inert atmosphere to obtain ternary blend solutions (40 mg ml^{-1}) with weight ratios of 1:1:x, where x is the weight ratio of SQ to P3HT, ranging from 0.5 to 5 wt%. For comparison, control devices with binary P3HT:PCBM BHJ films were made using the same procedure.

After fabrication, devices were illuminated at 100 mW cm^{-2} by a 150 W solar simulator with AM 1.5G filters (PV Measurements). The illumination intensity was determined by a NREL-calibrated silicon solar cell with KG-5 colour filter. All electrical measurements were carried out in air at room temperature. The active area of the device irradiated by the light was defined as 5 mm^2 by using a photomask, so no extra current outside the defined area was collected. Current density–voltage (J–V) curves were measured with a Keithley 2400 source measurement unit. The absorption spectra of dried films and solutions were obtained using a Varian Cary 3E UV-vis spectrophotometer. The EQE measurements were performed in air using a PV Measurements QEX7 system.

Ultrafast spectroscopy. Broadband TA spectra were obtained using an amplified Ti:sapphire laser system (Tsunami, Spectra Physics) and optical parametric amplifier (OPA). Briefly, neat P3HT and P3HT:SQ films were resonantly excited with ~100 fs laser pulses generated by the OPA at a repetition rate of 1 kHz. Time-resolved absorption spectra were obtained using a broadband supercontinuum probe pulse overlapped in time and space with the femtosecond pump pulse. The supercontinuum was produced by focusing a small portion of the amplified laser fundamental into a sapphire plate. Multiwavelength transient spectra were recorded using dual spectrometers (signal and reference) equipped with fast silicon array detectors. In all our experiments, the fluence value was held constant at 8 μJ cm^{-2} to rule out effects from exciton–exciton elimination as a result of high-power excitation. Chirping due to dispersion in the white probe beam was corrected before data analysis. Fluorescence decay kinetics was measured using the upconversion technique. Briefly, a femtosecond laser pulse from the OPA was used to resonantly excite a sample. The spontaneous emission was collected and mixed with a second 'gate' pulse in a nonlinear crystal optimized for sum frequency generation (SFG). The magnitude of the upconverted SFG signal was detected as a function of delay between the excitation and gate pulses. The time resolution of this method was measured to be ~250 fs.

Received 15 December 2012; accepted 7 March 2013; published online 5 May 2013

References

1. Krebs, F. C., Gevorgyan, S. A. & Alstrup, J. A roll-to-roll process to flexible polymer solar cells: model studies, manufacture and operational stability studies. *J. Mater. Chem.* **19,** 5442–5451 (2009).
2. Krebs, F. C. *et al.* A complete process for production of flexible large area polymer solar cells entirely using screen printing—first public demonstration. *Solar Ener. Mater. Solar Cells* **93,** 422–441 (2009).
3. Tipnis, R. *et al.* Large-area organic photovoltaic module—fabrication and performance. *Solar Ener. Mater. Solar Cells* **93,** 442–446 (2009).
4. Li, G., Zhu, R. & Yang, Y. Polymer solar cells. *Nature Photon.* **6,** 153–161 (2012).
5. Li, G. *et al.* High-efficiency solution processable polymer photovoltaic cells by self-organization of polymer blends. *Nature Mater.* **4,** 864–868 (2005).
6. Ma, W. L., Yang, C. Y., Gong, X., Lee, K. & Heeger, A. J. Thermally stable, efficient polymer solar cells with nanoscale control of the interpenetrating network morphology. *Adv. Funct. Mater.* **15,** 1617–1622 (2005).
7. Irwin, M. D., Buchholz, B., Hains, A. W., Chang, R. P. H. & Marks, T. J. P-type semiconducting nickel oxide as an efficiency-enhancing anode interfacial layer in polymer bulk-heterojunction solar cells. *Proc. Natl Acad. Sci. USA* **105,** 2783–2787 (2008).
8. Huang, J.-S., Chou, C.-Y. & Lin, C.-F. Efficient and air-stable polymer photovoltaic devices with WO_3–V_2O_5 mixed oxides as anodic modification. *IEEE Electron. Dev. Lett.* **31,** 332–334 (2010).
9. Bundgaard, E. & Krebs, F. C. Low band gap polymers for organic photovoltaics. *Solar Ener. Mater. Solar Cells* **91,** 954–985 (2007).
10. Kroon, R., Lenes, M., Hummelen, J. C., Blom, P. W. M. & de Boer, B. Small bandgap polymers for organic solar cells (polymer material development in the last 5 years). *Polym. Rev.* **48,** 531–582 (2008).
11. Lee, J. K. *et al.* Processing additives for improved efficiency from bulk heterojunction solar cells. *J. Am. Chem. Soc.* **130,** 3619–3623 (2008).
12. Park, S. H. *et al.* Bulk heterojunction solar cells with internal quantum efficiency approaching 100%. *Nature Photon.* **3,** 297–302 (2009).
13. Moon, J. S. *et al.* Effect of processing additive on the nanomorphology of a bulk heterojunction material. *Nano Lett.* **10,** 4005–4008 (2010).
14. Lou, S. J. *et al.* Effects of additives on the morphology of solution phase aggregates formed by active layer components of high-efficiency organic solar cells. *J. Am. Chem. Soc.* **133,** 20661–20663 (2011).
15. Peet, J., Senatore, M. L., Heeger, A. J. & Bazan, G. C. The role of processing in the fabrication and optimization of plastic solar cells *Adv. Mater.* **21,** 1521–1527 (2009).
16. Kirchartz, T., Taretto, K. & Rau, U. Efficiency limits of organic bulk heterojunction solar cells. *J. Phys. Chem. C* **113,** 17958–17966 (2009).
17. Hardin, B. E., Snaith, H. J. & McGehee, M. D. The renaissance of dye-sensitized solar cells. *Nature Photon.* **6,** 162–169 (2012).
18. Hardin, B. E. *et al.* Increased light harvesting in dye-sensitized solar cells with energy relay dyes. *Nature Photon.* **3,** 406–411 (2009).
19. Driscoll, K. *et al.* Enhanced photoresponse in solid-state excitonic solar cells via resonant energy transfer and cascaded charge transfer from a secondary absorber. *Nano Lett.* **10,** 4981–4988 (2010).
20. Hardin, B. E. *et al.* High excitation transfer efficiency from energy relay dyes in dye-sensitized solar cells. *Nano Lett.* **10,** 3077–3083 (2010).
21. Mor, G. K. *et al.* High-efficiency Förster resonance energy transfer in solid-state dye sensitized solar cells. *Nano Lett.* **10,** 2387–2394 (2010).
22. Mor, G. K. *et al.* Visible to near-infrared light harvesting in TiO_2 nanotube array-P3HT based heterojunction solar cells. *Nano Lett.* **9,** 4250–4257 (2009).
23. Chen, Y.-C., Hsu, C.-Y., Lin, R., Ho, K.-C. & Lin, J. Materials for the active layer of organic photovoltaics: ternary solar cell approach. *ChemSusChem* **6,** 20–35 (2013).
24. Belcher, W. J., Wagner, K. I. & Dastoor, P. C. The effect of porphyrin inclusion on the spectral response of ternary P3HT:porphyrin:PCBM bulk heterojunction solar cells. *Solar Ener. Mater. Solar Cells* **91,** 447–452 (2007).

25. Cooling, N. *et al.* A study of the factors influencing the performance of ternary MEH-PPV:porphyrin:PCBM heterojunction devices: a steric approach to controlling charge recombination. *Solar Ener. Mater. Solar Cells* **95,** 1767–1774 (2011).
26. Koppe, M. *et al.* Near IR sensitization of organic bulk heterojunction solar cells: towards optimization of the spectral response of organic solar cells. *Adv. Funct. Mater.* **20,** 338–346 (2010).
27. Honda, S., Ohkita, H., Benten, H. & Ito, S. Selective dye loading at the heterojunction in polymer/fullerene solar cells. *Adv. Ener. Mater.* **1,** 588–598 (2011).
28. Ameri, T. *et al.* Performance enhancement of the P3HT/PCBM solar cells through NIR sensitization using a small-bandgap polymer. *Adv. Ener. Mater.* **2,** 1198–1202 (2012).
29. Yang, L., Zhou, H., Price, S. C. & You, W. Parallel-like bulk heterojunction polymer solar cells. *J. Am. Chem. Soc.* **134,** 5432–5435 (2012).
30. Lobez, J. M., Andrew, T. L., Bulović, V. & Swager, T. M. Improving the performance of P3HT–fullerene solar cells with side-chain-functionalized poly(thiophene) additives: a new paradigm for polymer design. *ACS Nano* **6,** 3044–3056 (2012).
31. Silvestri, F. *et al.* Efficient squaraine-based solution processable bulk-heterojunction solar cells. *J. Am. Chem. Soc.* **130,** 17640–17641 (2008).
32. Wei, G. *et al.* Functionalized squaraine donors for nanocrystalline organic photovoltaics. *ACS Nano* **6,** 972–978 (2012).
33. Kim, Y. *et al.* A strong regioregularity effect in self-organizing conjugated polymer films and high-efficiency polythiophene:fullerene solar cells. *Nature Mater.* **5,** 197–203 (2006).
34. Lakowicz, J. R. in *Principles of Fluorescence Spectroscopy* Ch.13 (Springer, 2006).
35. Sapsford, K. E., Berti, L. & Medintz, I. L. Materials for fluorescence resonance energy transfer analysis: beyond traditional donor–acceptor combinations. *Angew. Chem. Int. Ed.* **45,** 4562–4589 (2006).
36. Sheng, C. X., Tong, M., Singh, S. & Vardeny, Z. V. Experimental determination of the charge/neutral branching ratio η in the photoexcitation of π-conjugated polymers by broadband ultrafast spectroscopy. *Phys. Rev. B* **75,** 085206 (2007).
37. Handlin, D. L. & Thomas, E. L. Visualization of ordered spherical microdomains of block copolymers by phase contrast electron microscopy. *J. Mater. Sci.* **3,** 137–140 (1984).
38. van Bavel, S. S., Bärenklau, M., de With, G., Hoppe, H. & Loos, J. P3HT/PCBM bulk heterojunction solar cells: impact of blend composition and 3D morphology on device performance. *Adv. Funct. Mater.* **20,** 1458–1463 (2010).
39. Xie, Y. *et al.* Femtosecond time-resolved fluorescence study of P3HT/PCBM blend films. *J. Phys. Chem C* **114,** 14590–14600 (2010).
40. Huang, J.-H., Chien, F.-C., Chen, P., Ho, K.-C. & Chu, C.-W. Monitoring the 3D nanostructures of bulk heterojunction polymer solar cells using confocal lifetime imaging. *Anal. Chem.* **82,** 1669–1673 (2010).
41. Marsh, R. A., Hodgkiss, J. M., Albert-Seifried, S. & Friend, R. H. Effect of annealing on P3HT:PCBM charge transfer and nanoscale morphology probed by ultrafast spectroscopy. *Nano Lett.* **10,** 923–930 (2010).
42. Tian, M. *et al.* Search for squaraine derivatives that can be sublimed without thermal decomposition. *J. Phys. Chem. B* **106,** 4370–4376 (2002).

Acknowledgements

This work was supported primarily by the SOLAR program of the National Science Foundation (NSF; DMR-0934520) and the Yale Climate and Energy Institute. A.D.T. acknowledges support from a NSF-CAREER award (CBET-0954985) and NASA (CT Space Grant Consortium). Research was carried out in part at the Centre for Functional Nanomaterials, Brookhaven National Laboratory, which is supported by the US Department of Energy, Office of Basic Energy Sciences (contract no. DE-AC02-98CH10886). The authors thank C. Schmuttenmaer, E. Yan and S. Wang for informative discussions.

Author contributions

J.-S.H. and A.D.T. conceptualized the project. J.-S.H. designed and performed the device experiments and data analysis. J.-S.H., T.G. and M.Y.S. performed the ultrafast experiments and resulting data analysis. J.-S.H., T.G. and X.L. performed TEM experiments. J.-S.H., S.T. and M.L. performed the EQE experiments. E.A.B. and N.H. synthesized the SQ dye. A.D.T and J.-S.H. laid out the design of the manuscript. J.-S.H. wrote the original manuscript and all authors contributed equally towards improving it.

Additional information

Supplementary information is available in the online version of the paper. Reprints and permissions information is available online at www.nature.com/reprints. Correspondence and requests for materials should be addressed to A.D.T.

Competing financial interests

The authors declare no competing financial interests.